HHS Public Access

Author manuscript

Mol Immunol. Author manuscript; available in PMC 2017 October 01.

Published in final edited form as:

Mol Immunol. 2016 October ; 78: 79–88. doi:10.1016/j.molimm.2016.08.012.

L-Plastin promotes podosome longevity and supports macrophage motility

Julie Y. Zhou[a,1], **Taylor P. Szasz**[a], **Phillip J. Stewart-Hutchinson**[a], **Janardan Sivapalan**[a], **Elizabeth M. Todd**[a], **Lauren E. Deady**[a], **John A. Cooper**[b], **Michael D. Onken**[b], and **S. Celeste Morley**[a,c,*]

[a] Department of Pediatrics, Division of Infectious Diseases, Washington University School of Medicine, St. Louis, MO, 63110, United States

[b] Department of Biochemistry and Molecular Biophysics, Washington University School of Medicine, St. Louis, MO, 63110, United States

[c] Department of Pathology and Immunology, Division of Immunobiology, Washington University School of Medicine, St. Louis, MO, 63110, United States

Abstract

Elucidating the molecular regulation of macrophage migration is essential for understanding the patho-physiology of multiple human diseases, including host responses to infection and autoimmune disorders. Macrophage migration is supported by dynamic rearrangements of the actin cytoskeleton, with formation of actin-based structures such as podosomes and lamellipodia. Here we provide novel insights into the function of the actin-bundling protein L-plastin (LPL) in primary macrophages. We found that podosome stability is disrupted in primary resident peritoneal macrophages from $LPL^{-/-}$ mice. Live-cell imaging of F-actin using resident peritoneal macrophages from LifeACT-RFP^{+} mice demonstrated that loss of LPL led to decreased longevity of podosomes, without reducing the number of podosomes initiated. Additionally, macrophages from $LPL^{-/-}$ mice failed to elongate in response to chemotactic stimulation. These deficiencies in podosome stabilization and in macrophage elongation correlated with impaired macrophage transmigration in culture and decreased monocyte migration into murine peritoneum. Thus, we have identified a role for LPL in stabilizing long-lived podosomes and in enabling macrophage motility.

* Corresponding author at: Department of Pediatrics, Division of Infectious Diseases, Washington University School of Medicine, St. Louis, MO, 63110, United States. morley c@kids.wustl.edu (S.C. Morley).

[1]Present address: Case Western Reserve University, Cleveland, OH, 44106, United States.

Author contributions

JYZ and TPS were primarily responsible for the execution and interpretation of the experiments and contributed significantly to experimental design and manuscript preparation. PJSH, JS, EMT, LED, and MDO provided significant contributions to the execution and interpretation of experimental results. JAC contributed to the data interpretation and manuscript preparation. SCM was responsible for the conception, design, and interpretation of experiments and primarily responsible for manuscript preparation.

Appendix A. Supplementary data

Supplementary data associated with this article can be found, in the online version, at http://dx.doi.org/10.1016/j.molimm.2016.08.012.

Keywords

Actin cytoskeleton; L-plastin; Podosomes; Macrophages; Cell motility

1. Introduction

Macrophage and monocyte migration is critical to host immunity and health (Friedl and Weigelin, 2008; Pollard, 2009). Multiple actin-based structures, including podosomes and lamellipodia, support macrophage migration. (Linder and Aepfelbacher, 2003; Calle et al., 2006). Podosomes are defined as cores of F-actin surrounded by adhesion-associated proteins, including vinculin and paxillin. Podosomes serve as anchors for migrating cells interacting on substrate, and they promote the assembly and function of macromolecular signaling complexes (Calle et al., 2006). Macrophages polarize and elongate following chemotactic stimulation, generating broad, flat lamellipodia at the leading edge (Abshire et al., 2011). Despite decades of research detailing the structure and function of lamellipodia and podosomes, the complex interplay of actin-related proteins that generate and regulate these structures has not been fully elucidated.

Here, we focus on the role of the actin-bundling protein L-plastin (LPL; gene: Lymphocyte cytosolic protein 1, *LCP1*) in macrophage motility. Initial studies of $LPL^{-/-}$ mice found no defects in neutrophil motility, adhesion and spreading, and no apparent disruption of bone marrow-derived macrophage morphology (Chen et al., 2003). However, two recent lines of evidence suggest that LPL may indeed play an important role in monocyte/macrophage migration. First, in lymphocytes, LPL was found to be required for polarization, lamellipodia formation, and motility (Morley et al., 2010; Todd et al., 2011; Freeley et al., 2012; Dubovsky et al., 2013). Second, in a macrophage cell line, anti-LPL nanobodies that inhibit binding of LPL to F-actin led to decreases in podosome stability and matrix invasion (De Clercq et al., 2013). To reconcile these apparently disparate reports, and to advance our knowledge of the function of LPL in macrophage biology, we investigated podosome formation and duration, along with cell polarization and migration, using primary resident macrophages from mice lacking LPL.

2. Materials and methods

2.1. Mice

$LPL^{-/-}$ mice have been described (Morley et al., 2010). LifeAct-RFP^{+} mice (Riedl et al., 2008; Riedl et al., 2010) were obtained from Klaus Ley, Ph.D., La Jolla Research Institute. Mice were co-housed in specific-pathogen-free barrier animal facilities at Washington University School of Medicine (WUSM). Animal experiments were approved by the WUSM Institutional Animal Care and Use Committee.

2.2. Medium

Cells were cultured in D10 medium (Dulbecco's modified Eagle Medium [DMEM; Hyclone Laboratories, South Logan, UT] with 10% fetal calf serum [FCS; GE Healthcare Life Sciences/Hyclone, Pittsburgh, PA], 10 mM HEPES [Hyclone], 1X MEM nonessential acids

[Mediatech, Manassas, VA], 1 mM sodium pyruvate [Mediatech], 1X penicillin/streptomycin [Life Technologies, Grand Island, NY], 50 μM 2-ME [Sigma-Aldrich, St. Louis, MO], and 1X L-glutamine [GlutaMax, Invitrogen, Carlsbad, CA]. Reduced serum media was as above except with 0.5% FCS.

2.3. Cell isolation

Peritoneal macrophages were harvested by adherence to 60-mm culture dishes (2 h at 37 °C and 5% CO_2) after peritoneal lavage (Zhang et al., 2008; Ray and Dittel, 2010). CCR2 is equivalently expressed on peritoneal macrophages (10–20%) and monocytes (100%) from WT and $LPL^{-/-}$ mice (data not shown).

2.4. Confocal microscopy

Cells were incubated on glass coverslips (Electron Microscopy Sciences, Hatfield, PA) and serum-starved for 2 h prior to chemotactic stimulation for 30 min (D10 + CCL2 (100 ng/ml; Shenandoah Biotechnology, Warwick, PA)) or CXCL12 (1 μg/ml; R&D Systems). Cells were fixed (4% paraformaldehyde), permeabilized with 0.5% Triton X-100 (Sigma), blocked in 5% normal goat serum (Vector Laboratories, Burlingame, CA), then stained with anti-vinculin mAb (Santa Cruz Biotechnology, Dallas, TX), anti-paxillin mAb (BD Biosciences), or anti-LPL mAb (Morley et al., 2010). The secondary anti-mouse antibody was conjugated to DyLight594 (Jackson ImmunoResearch Laboratories, West Grove, PA) or Alex-aFluor568 (Invitrogen). F-actin was imaged by staining with phalloidin-AlexaFluor 488 (Invitrogen). Samples were viewed with an Olympus FV1000 confocal microscope with 20× air and 60× oil objectives. Images were obtained using synchronized scanning with a multiline argon laser (457 nm, 488 nm, and 514 nm) and a 635-nm diode laser using FV10-ASW 3.0 software. Additional imaging (Fig. 2C) was performed at the Washington University Center for Cellular Imaging (WUCCI), using a Nikon A1R scanning confocal microscope with a 100× oil immersion objective utilizing 405 nm, 488 nm, and 561 nm laser lines using NIS-Elements software.

Intensity profile analyses were generated in ImageJ (National Institutes of Health, Bethesda, MD; http://imagej.nih.gov/ij/), using the plot profile algorithm that calculates intensity statistics from pixel values (Hartig, 2013). Relative intensities of fluorescence were plotted versus the lengths of lines drawn through podosomes on image stacks. The circularity of cells was determined using the built-in ImageJ circularity index, scaled from “0” (linear) to “1” (perfectly circular).

2.5. Live cell imaging

Macrophages isolated from naive LifeACT-RFP^{+}-WT and $LPL^{-/-}$ mice were placed on coverslips pre-treated with Rat Tail Collagen 1 (BD Biosciences, 47.3 μg/ml in acetic acid). Cells were serum-starved for 1 h and then re-exposed to serum immediately prior to imaging. Images were collected from the first cell in which podosomes appeared. Cells were imaged for 30 min, with two cells imaged consecutively after serum re-exposure. Images were acquired in the same z-plane every 15–20 s using an Olympus IX70 microscope with a 100×/1.4NA oil objective, a Yokogawa spinning-disk confocal scanning unit, and a Hamamatsu Orca Flash4 CMOS camera. Cells were maintained at 37 °C with 5.0% CO_2 in

a Tokai Hit humidified chamber. The microscope was controlled and images were acquired with Micro-Manager 1.4.22 and ImageJ software. Images were converted to videos with ImageJ, using the Images to Stack function with the Time Stamper plugin.

Videos records of podosome turnover were assessed by a blinded observer, and individual podosomes were tracked manually using ImageJ and the MTrackJ plugin. Podosome duration, total podosome counts, and intensity over time were calculated (TimeSeriesAnalyzer plugin). Heat maps of intensity over time were generated from the raw data with a script in the open-source software R (www.r-project.org/).

2.6. In vitro cell migration assays

In vitro cell migration assays were performed as described (Van Goethem et al., 2010; Green et al., 2012; Justus et al., 2014). Transwell inserts (5 μm, Corning CoStar, Lowell, MA) were coated with collagen (2.5 μg). For chemotactic stimulation, cells in the upper chamber were kept in reduced serum media and D10 + CCL2 was added to the lower chamber. Control samples were incubated in the absence of a gradient (D10 medium in both chambers) to maintain viability. Inserts were fixed in 4% paraformaldehyde, permeabilized with 100% methanol, and stained with 0.5% crystal violet (Acros Organics, Geel, Antwerpen, Belgium) (Justus et al., 2014). Two images representing 79% of the membrane area were captured for each membrane before (to quantify number of input cells) and after scraping the upper membrane (to remove non-transmigrated cells) using an Olympus BX60 microscope with an Olympus U Plan Fl 20× objective and Zeiss AxioCam camera using AxioVision software. Cells present on the insert before and after scraping were quantified using ImageJ's automated cell counting analysis tool (Abramoff et al., 2004; Schneider et al., 2012; Hartig, 2013) and by hand. The percentage of transmigrated cells was calculated from the numbers of cells present before and after scraping.

2.7. In vivo monocyte migration

One day after i.p. injection of either CCL2 (50 μg) in PBS or PBS alone, mice were sacrificed, and peritoneal lavage fluid was analyzed by flow cytometry using the following commercial antibodies: anti-B220- FITC, F4/80-PE, Ly-6C-PerCP/Cy5.5, CD11b-PE/Cy7, Ly-6G-PacBlue, (Biolegend, San Diego, CA); and CCR2-allophycocyanin (APC; Bio-Techne (formerly R&D Systems), Minneapolis, MN). Cell samples were pre-incubated with 1 μg Fc-block (2.4G2 hybridoma; ATCC, Manassas, VA). Samples were acquired with a Becton Dickinson FACScan (BD Biosciences) flow cytometer with DxP multi-color upgrades by Cytek Development Inc. (Woodland Park, NJ), and data were analyzed using FlowJo software (FlowJo LLC, Ashland, OR).

2.8. Histology

Hematoxylin and eosin: Spleens from WT or $LPL^{-/-}$ mice were fixed in 10% neutral buffered formalin and embedded in paraffin prior to sectioning and staining with hematoxylin and eosin by the Washington University core service. Immunofluorescence: Images of splenic follicles were prepared as previously described (Todd et al., 2011). In brief, spleens from WT or $LPL^{-/-}$ mice were frozen in OCT (Sakura Finetek, Torrance, CA), sectioned (8 μm) and fixed in acetone. B cell follicles were illuminated by staining with anti-

MOMA-1-FITC (Serotec, Raleigh, NC) and anti-IgM (eBioscience) followed by anti-rat IgG-AlexaFluor594 (Invitrogen). Slides were viewed with a Zeiss Axioskop equipped with a Zeiss Plan-Neufluar × 10 or ×20 objective or an Olympus BX60 equipped with an Olympus U Plan Fl ×20 objective. Images were acquired using a Zeiss AxioCam with Axiovision software. Brightness and contrast were uniformly adjusted in Adobe Photoshop (Todd et al., 2011).

2.9. Data analysis and statistics

Data were analyzed and graphed using Prism software (Graph-Pad, La Jolla, CA). Statistical tests did not assume normal distribution, unless noted otherwise, and P values were determined using unpaired, two-tailed Mann-Whitney tests.

3. Results

3.1. L-Plastin (LPL) is a key component of podosomes

Podosomes are characterized as foci of F-actin approximately 0.5–2 μm in diameter, concentrated toward the leading edge of migrating cells (De Clercq et al., 2013). First, we found that LPL colocalizes with F-actin in podosomes in thioglycollate-elicited peritoneal macrophages from WT mice (Fig. 1A, arrows), demonstrating that LPL is a component of podosomes in our system, as found in other cells (Babb et al., 1997; Evans et al., 2003; De Clercq et al., 2013). The positions of peaks of F-actin and LPL in line scan intensity profiles were essentially identical (Fig. 1B).

We next examined the requirement for LPL in podosome formation in serum-stimulated resident peritoneal macrophages. Based upon F-actin staining, fewer podosomes were found in macrophages from $LPL^{-/-}$ mice, compared to WT mice. Also, podosomes in LPL-deficient cells were poorly demarcated with diffuse borders (Fig. 1C, D, E). Our results are consistent with those of De Clercq et al. (De Clercq et al., 2013), who observed that inhibition of LPL actin-bundling activity with specific nanobodies resulted in fewer podosomes with a disrupted morphology (De Clercq et al., 2013). Here, we removed LPL completely from primary cells, using a genetic approach, and demonstrated that LPL is important for podosome formation.

3.2. LPL is not required for co-localization of paxillin and vinculin to podosomes in resident peritoneal macrophages

Podosomes are characterized by the accumulation of adhesion-associated proteins vinculin and paxillin with F-actin (Calle et al., 2006). To determine whether LPL helps to recruit vinculin and paxillin, we examined co-localization of vinculin and paxillin with F-actin in serum-stimulated peritoneal macrophages from WT and $LPL^{-/-}$ mice. We observed no difference in the degree of colocalization of F-actin with vinculin or paxillin (Fig. 2A, B) comparing WT and $LPL^{-/-}$ macrophages that had been stimulated with serum.

We also examined podosome formation in peritoneal macrophages following stimulation with the chemoattractant CXCL12, in the absence of serum (Fig. 2C). Podosomes formed following CXCL12 stimulation appeared smaller than those formed in the presence of serum

(Fig. 2C). Co-localization of paxillin or vinculin with F-actin punctae occurred equivalently in resident peritoneal macrophages from WT and LPL$^{-/-}$ mice (Fig. 2C, insets), although we observed less colocalization between vinculin or paxillin with F-actin overall (data not shown). Thus, LPL is not required for the association of vinculin and paxillin with F-actin in podosomes in resident peritoneal macrophages. Interestingly, in a parallel study in alveolar macrophages, a distinct primary macrophage lineage, F-actin did not co-localize with vinculin in the absence of LPL (Todd et al., manuscript submitted), suggesting that podosome composition and regulation may vary with macrophage type.

3.3. LPL promotes podosome longevity

Our finding of decreased numbers of podosomes, combined with normal levels of colocalization of vinculin and paxillin with F-actin, suggested that LPL may be dispensable for initiation of podosome assembly but required for podosome stability. To test this hypothesis, we measured podosome lifetimes in resident peritoneal macrophages isolated from LifeACT-RFP^{+}-WT and LifeACT-RFP^{+}-LPL$^{-/-}$ mice. Use of LifeACT-RFP^{+} mice allowed us to study primary resident macrophage cells that had not been subjected to pro-inflammatory stimuli, which is important because activation with pro-inflammatory stimuli, such as thioglycollate, is known to alter podosome morphology (Cougoule et al., 2012). Cells were serum-starved, then re-exposed to serum immediately prior to live-cell imaging. We imaged and tracked the position and fluorescence intensity of every identified podosome in each cell (arrows, Fig. 3A; Supplemental Movies 1 and 2).

Macrophages isolated from WT and LPL$^{-/-}$ mice initiated similar numbers of podosomes (Fig. 3B). For WT resident peritoneal macrophages, we observed a large number of short-lived (duration < 15 min) podosomes, with a smaller number of podosomes persisting for > 15 min. For macrophages from LPL$^{-/-}$ mice, podosome lifetimes were decreased overall compared to WT. The greatest difference was in the number of podosomes lasting > 15 min, which was 11.9% (158 of 1327) in WT cells versus 5.3% (61 of 1133) podosomes in LPL-deficient cells (Fig. 3C). An additional feature of podosome dynamics is that a single podosome may oscillate in fluorescence intensity, with cycles of increase and decrease, while remaining in the same position. This feature can be seen in the movies (Supplemental Movies 1 and 2). For one representative oscillating podosome, intensity vs time is plotted in Fig. 3D.

To visualize and compare the data for podosome duration and for oscillation of fluorescence intensity in multiple podosomes across multiple cells, we created a “heat map” display (Fig. 3D, E). In this representation, intensity is indicated by a color scale, with time represented by distance along the x-axis. An example of one “heat map” row is displayed above the intensity profile in Fig. 3D. Every podosome is thus represented by a row representing the fluorescence intensity over time, with each “block” of rows representing all the podosomes for a given cell (Fig. 3E). Overall, the results reveal that podosome formation, duration and oscillation display extensive heterogeneity across the population of resident primary macrophages. Podosome intensity and duration are greater in WT macrophages compared to LPL-deficient macrophages, seen most clearly from the number of podosomes persisting after 30 min (Fig. 3E). This result accounts for our observation of decreased numbers of

podosomes in fixed-cell preparations (Fig. 1D). Our results indicate that LPL promotes the stability and persistence of F-actin at podosomes.

3.4. LPL supports macrophage polarization and migration

Chemotactic stimulation of macrophages induces an elongated morphology; cells polarize and generate lamellipodia (Evans and Falke, 2007; Abshire et al., 2011). To investigate the role of LPL in chemotactic response, we examined the morphology of resident peritoneal macrophages from WT and $LPL^{-/-}$ mice after chemotactic stimuli (Fig. 4A). WT macrophages adopted an elongated phenotype, an effect that we quantified by calculating circularity index (see Methods) (Fig. 4B). In contrast, macrophages from $LPL^{-/-}$ mice failed to elongate and showed no change in circularity index. Thus, LPL has a critical function in the support of macrophage elongation, which is similar to the role of LPL in T cell polarization (Morley et al., 2010; Freeley et al., 2012).

To determine whether LPL is important for macrophage migration, we counted cells migrating across collagen-coated Transwell membranes in response to a chemotactic gradient (Fig. 4C). For WT cells, a chemoattractant gradient significantly increased the proportion of resident peritoneal macrophages migrating across collagen (Fig. 4D), consistent with previous results (Cougoule et al., 2012). In contrast, migration of macrophages from $LPL^{-/-}$ mice did not increase on exposure to a chemotactic gradient (Fig. 4C, D). Thus, LPL is important for migration of resident primary macrophages *in vitro*.

We extended our observations of cell migration to whole animals by quantifying the accumulation of monocytes in the peritoneal cavity after i.p. injection of the chemoattractant CCL2. Monocytes were counted in peritoneal lavage fluid by flow cytometry, defined as $CD11b^{+}F4/80^{int}Ly6C^{+}CCR2^{+}$ cells (Fig. 4E). Few monocytes were present in peritoneal lavage from control animals. CCL2 treatment induced the migration of monocytes into the peritoneum in WT mice, and this effect was significantly blunted in $LPL^{-/-}$ mice (Fig. 4F), providing an *in vivo* correlate of the transmigration defect observed in culture. Thus, we demonstrate a requirement for LPL in the migration of myeloid cells in vitro and in vivo, one that is associated with requirements for LPL in podosome longevity and cellular elongation.

3.5. Reduced macrophage migration does not affect the histologic architecture of the spleen

The spleen is essential to the rapid clearance of bloodborne pathogens (Borges da Silva et al., 2015). The splenic microarchitecture facilitates the filtering of the blood, with capture of foreign particles and antigen delivery. The spleen is divided into the red pulp, containing sinusoids, and the white pulp, encompassing the lymphoid follicles. The marginal zone forms the border between the red and white pulp. Several macrophage subpopulations, including marginal metallophilic macrophages (MMM) and marginal zone macrophages (MZM), establish the marginal zone and participate in antigen capture and delivery. Chemokine signaling supports the correct patterning of splenic architecture (Forster et al., 1999). To determine whether impaired macrophage migration impacted the formation of the marginal zone of the spleen, splenic sections from WT and $LPL^{-/-}$ mice were examined

(Fig. 5). Histology of spleens from LPL$^{-/-}$ revealed apparently normal architecture, with clear division into red pulp and the denser lymphoid follicles. Immunofluorescence of frozen sections revealed distinct lymphoid follicles surrounded by MOMA-1^{+} macrophages. Thus, impaired migration of macrophages does not appear to result in grossly abnormal splenic architecture (Fig. 5).

4. Discussion

Here we demonstrate for the first time a requirement for LPL in the migration of resident monocytes and macrophages. Resident peritoneal macrophages from LPL$^{-/-}$ mice failed to transmigrate across collagen-coated Transwell inserts *in vitro*, and monocytes did not migrate into the peritoneal space following *in vivo* CCL2 challenge of LPL$^{-/-}$ mice (Fig. 4). The dependence of monocyte/macrophage migration upon LPL could not be predicted in advance, because LPL has been previously shown to be dispensable for neutrophil migration (Chen et al., 2003), albeit essential for normal lymphocyte motility (Lin et al., 2010; Morley et al., 2010; Todd et al., 2011; Freeley et al., 2012; Dubovsky et al., 2013).

LPL-mediated support of at least two different F-actin dependent biological processes, podosome longevity and cell polarization, could explain the requirement for LPL in normal migration of resident peritoneal macrophages. First, we found that LPL is important for podosome longevity (Fig. 3). Podosomes are small, circular, adhesion-based accumulations of actin-binding and signaling proteins linked to F-actin found predominantly in cells of myeloid origin, including monocytes, macrophages, dendritic cells and osteoclasts (Williams and Ridley, 2000; Linder and Wiesner, 2015). LPL has been previously shown to be a component of macrophage podosomes, but the function of LPL in assembling or maintaining this actin-based structure has been explored in only a few reports (Messier et al., 1993; Babb et al., 1997; Evans et al., 2003; Ma et al., 2010; De Clercq et al., 2013). Tight temporal correlation of LPL with F-actin as podosomes formed, disassembled, and reformed in the IC-21 macrophage cell line suggested that LPL provided structural support to podosome-associated actin (Evans et al., 2003). Inhibition of actin binding by LPL through generation of camelid nanobodies in THP-1-differentiated macrophages resulted in diffuse, poorly-formed podosomes with shorter half-lives (De Clercq et al., 2013). Finally, LPL was noted to be key component of actin aggregates in the early stages of osteoclast sealing ring formation, and it was suggested that LPL-supported actin aggregates served to assemble signaling complexes independently of integrin-mediated signaling (Ma et al., 2010). Beyond these three studies, two of which were performed in cell lines, the function of LPL in podosome formation or maintenance had been uncharacterized.

Using a genetic approach in primary cells, we advanced the conclusions from the previous studies by demonstrating reduced podosome longevity in the absence of LPL. We first showed that resident peritoneal macrophages from LPL$^{-/-}$ mice exhibited fewer podosomes in images of fixed cells, and that those podosomes were relatively diffuse with poorly-defined borders, similar to the effects observed with anti-LPL nanobodies (Fig. 1) (Evans et al., 2003). We extended these observations by showing that initiation of podosome formation was intact, in that similar numbers of podosomes were identified in live-cell imaging of resident peritoneal macrophages from LifeAct-RFP^{+} WT and LPL$^{-/-}$ mice (Fig. 3B). In

addition, accumulation of the integrin-binding proteins vinculin and paxillin to F-actin punctae did not require LPL (Fig. 2). However, the podosomes that formed in resident peritoneal macrophages lacking LPL were not maintained, with a significant reduction in half-life. Furthermore, fewer podosomes demonstrated oscillations of fluorescence intensity over time in the absence of LPL (Fig. 3E). Thus, we speculate that the finding of destabilization of podosomes in the absence of LPL could explain the observation of impaired migration of resident primary macrophages and monocytes lacking LPL.

Second, LPL was also required for macrophage elongation following chemotactic stimulation (Fig. 4A). Polarization and generation of a leading and trailing edge is required for directed cell migration. Macrophages stimulated to migrate generate leading and trailing edges, elongating in the direction of movement (Evans and Falke, 2007; Abshire et al., 2011; Lam and Huttenlocher, 2013). Polarization towards the chemotactic stimulus depends on dynamic rearrangements of F-actin. Failure of macrophages from $LPL^{-/-}$ mice to elongate is reminiscent of the failure of T cells from $LPL^{-/-}$ mice to polarize in response to chemotactic cues (Morley et al., 2010) and to generate lamellipodia (Freeley et al., 2012). Loss of the ability to generate leading and trailing edges, seen in cells lacking LPL, could result in defective cell motility and migration.

The requirement for LPL in leukocyte migration may vary with cell lineage. We observed decreased recruitment of LPL-deficient monocytes after i.p. injection with CCL2, but we did not observe macrophage migration defects in $LPL^{-/-}$ mice following i.p. injection of thioglycollate, a highly inflammatory stimulus (data not shown). Thioglycollate elicits inflammatory macrophages, which are capable of migrating through dense Matrigel, while naive monocytes and resident peritoneal macrophages are not (Cougoule et al., 2012). Additionally, the requirement for LPL in leukocyte motility may depend upon the extrinsic environment through which the cell moves. In other results examining alveolar macrophages, we found a substantial defect in monocyte transmigration in response to intratracheal CCL2 (Todd et al., manuscript submitted) in $LPL^{-/-}$ mice compared to WT mice. Our findings highlight the importance of systematically analyzing requirements for actin-binding proteins in the support of cell motility in multiple lineages and environments.

Our knowledge of the function of LPL in macrophage/monocyte motility may be relevant to elucidation of cellular mechanisms underlying cancer metastasis. While LPL is not normally expressed outside cells of the immune system, over half of epithelial carcinomas and non-epithelial mesenchymal tumors examined ectopically expressed LPL (Delanote et al., 2005). Moreover, phosphorylation of LPL is associated with metastasis (Riplinger et al., 2014), and variant alleles of LPL have been associated with cancer progression (Ning et al., 2014). Recently, it has been shown that depletion of LPL can inhibit tissue invasion by prostate cancer cell lines, and ectopic expression of LPL can increase the metastatic potential of melanoma lines (Riplinger et al., 2014). Macrophage podosomes resemble cancer cell invadopodia in certain ways, so improved understanding of the function of LPL in podosome biology may reveal new targets for prevention of cancer metastasis.

The physiological consequence of reduced monocyte and macrophage migration in $LPL^{-/-}$ mice is an open area of active investigation. Chemokine signaling is required for the correct

patterning of lymphoid organs and tissue remodeling, as evidenced by the disruption of tissue architecture in mice lacking chemokine receptors such as CXCR4 and CCR7 (Tachibana et al., 1998; Forster et al., 1999; Allen et al., 2004). We did not find evidence that the motility defect of macrophages resulted in disrupted splenic architecture in $LPL^{-/-}$ mice (Fig. 5; (Todd et al., 2011)), suggesting that chemokine receptor signaling to tissue patterning can be dissociated from the cytoskeletal rearrangements required for cellular migration (Morley et al., 2010). The spleen functions to generate rapid immune response to bloodborne pathogens, such as *Streptococcus pneumoniae* (Borges da Silva et al., 2015). While splenic architecture appears to be normal, $LPL^{-/-}$ mice exhibited a delayed early IgM response to heat-killed pneumococcal antigen (Todd et al., 2011), suggesting functional impairment of either antigen delivery or lymphocyte activation. We previously found a correlation between diminished anti-pneumococcal response and decreased numbers of marginal zone B cells in $LPL^{-/-}$ mice, but our current data may prompt a re-examination of the interplay between marginal zone B cells and macrophages in $LPL^{-/-}$ mice (Todd et al., 2011).

In summary, our results are the first to show a requirement for LPL in podosome longevity in primary resident macrophages. Our studies demonstrate the utility of $LifeACT\text{-}RFP^{+}$ mice for imaging actin dynamics in resident primary cells. Different cell types organize actin in different ways, and actin reorganization may vary with cell stimulus and context, and therefore the ability to directly observe actin dynamics in resident immune cells will provide a more physiological understanding of the mechanics of cell motility. Furthermore, LPL is required in a cell-specific manner for cell migration. Future analysis of the function of LPL in supporting cell polarity and podosome formation will reveal clinically relevant insights into spatiotemporal regulation of cell motility.

Supplementary Material

Refer to Web version on PubMed Central for supplementary material.

Acknowledgements

We would like to thank Darren Kreamalmeyer for his technical assistance with the maintenance of our mouse colony. The anti-LPL mAb was provided by Eric J. Brown (Morley et al., 2010). We would like to thank Mary Dinauer for critical review of the manuscript and Kristine Wylie for assistance with generation of the heat map.

Supported by a grant from NIAID/NIH [R01AI104732-02], a Basil O'Connor Award from the March of Dimes, a Grant-in-Aid from the American Heart Association, and a Biomedical Research Grant from the American Lung Association to SCM. This work was also supported by funds from the Children's Discovery Institute in Saint Louis [MD-FR-2010-83] to SCM. MDO, JAC, and live-cell imaging experiments were supported by NIH grants GM95509, GM38542 and GM118171 to JAC. WUCCI is supported by funding provided by the Children's Discovery Institute of Washington University and St. Louis Children's Hospital.

Abbreviations

APC	allophycocyanin
D10	Dulbecco's modified Eagle Medium with 10% FCS
LPL	L-plastin

References

Abramoff MD, Magalhaes PJ, Ram SJ. Image processing with image. J. Biophotonics Int. 2004; 11:36–42.

Abshire MY, Thomas KS, Owen KA, Bouton AH. Macrophage motility requires distinct alpha5beta1/FAK and alpha4beta1/paxillin signaling events. J. Leukoc. Biol. 2011; 89:251–257. [PubMed: 21084629]

Allen CD, Ansel KM, Low C, Lesley R, Tamamura H, Fujii N, Cyster JG. Germinal center dark and light zone organization is mediated by CXCR4 and CXCR5. Nat. Immunol. 2004; 5:943–952. [PubMed: 15300245]

Babb SG, Matsudaira P, Sato M, Correia I, Lim SS. Fimbrin in podosomes of monocyte-derived osteoclasts. Cell Motil. Cytoskeleton. 1997; 37:308–325. [PubMed: 9258504]

Borges da Silva H, Fonseca R, Pereira RM, Cassado Ados A, Alvarez JM, D'Imperio Lima MR. Splenic macrophage subsets and their function during blood-borne infections. Front. Immunol. 2015; 6:480. [PubMed: 26441984]

Calle Y, Burns S, Thrasher AJ, Jones GE. The leukocyte podosome. Eur. J. Cell Biol. 2006; 85:151–157. [PubMed: 16546557]

Chen H, Mocsai A, Zhang H, Ding RX, Morisaki JH, White M, Rothfork JM, Heiser P, Colucci-Guyon E, Lowell CA, et al. Role for plastin in host defense distinguishes integrin signaling from cell adhesion and spreading. Immunity. 2003; 19:95–104. [PubMed: 12871642]

Cougoule C, Van Goethem E, Le Cabec V, Lafouresse F, Dupre L, Mehraj V, Mege JL, Lastrucci C, Maridonneau-Parini I. Blood leukocytes and macrophages of various phenotypes have distinct abilities to form podosomes and to migrate in 3D environments. Eur. J. Cell Biol. 2012; 91:938–949. [PubMed: 22999511]

De Clercq S, Boucherie C, Vandekerckhove J, Gettemans J, Guillabert A. l-Plastin nanobodies perturb matrix degradation, podosome formation, stability and lifetime in THP-1 macrophages. PLoS One. 2013; 8:e78108. [PubMed: 24236012]

Delanote V, Vandekerckhove J, Gettemans J. Plastins: versatile modulators of actin organization in (patho)physiological cellular processes. Acta Pharmacol. Sin. 2005; 26:769–779. [PubMed: 15960882]

Dubovsky JA, Chappell DL, Harrington BK, Agrawal K, Andritsos LA, Flynn JM, Jones JA, Paulaitis ME, Bolon B, Johnson AJ, et al. Lymphocyte cytosolic protein 1 is a chronic lymphocytic leukemia membrane-associated antigen critical to niche homing. Blood. 2013; 122:3308–3316. [PubMed: 24009233]

Evans JH, Falke JJ. Ca2+ influx is an essential component of the positive-feedback loop that maintains leading-edge structure and activity in macrophages. Proc. Natl. Acad. Sci. U. S. A. 2007; 104:16176–16181. [PubMed: 17911247]

Evans JG, Correia I, Krasavina O, Watson N, Matsudaira P. Macrophage podosomes assemble at the leading lamella by growth and fragmentation. J. Cell Biol. 2003; 161:697–705. [PubMed: 12756237]

Forster R, Schubel A, Breitfeld D, Kremmer E, Renner-Muller I, Wolf E, Lipp M. CCR7 coordinates the primary immune response by establishing functional microenvironments in secondary lymphoid organs. Cell. 1999; 99:23–33. [PubMed: 10520991]

Freeley M, O'Dowd F, Paul T, Kashanin D, Davies A, Kelleher D, Long A. l-Plastin regulates polarization and migration in chemokine-stimulated human T lymphocytes. J. Immunol. 2012; 188:6357–6370. [PubMed: 22581862]

Friedl P, Weigelin B. Interstitial leukocyte migration and immune function. Nat. Immunol. 2008; 9:960–969. [PubMed: 18711433]

Green TD, Park J, Yin Q, Fang S, Crews AL, Jones SL, Adler KB. Directed migration of mouse macrophages in vitro involves myristoylated alanine-rich C-kinase substrate (MARCKS) protein. J. Leukoc. Biol. 2012; 92:633–639. [PubMed: 22623357]

Hartig SM. Ausubel, Frederick M.Basic image analysis and manipulation in ImageJ. Curr. Prot. Mol. Biol. 2013 Chapter 14, Unit14 15.

Justus, CR.; Leffler, N.; Ruiz-Echevarria, M.; Yang, LV. In vitro cell migration and invasion assays.. J. Vis. Exp. 2014. http://dx.doi.org/10.3791/51046

Lam PY, Huttenlocher A. Interstitial leukocyte migration in vivo. Curr. Opin. Cell Biol. 2013; 25:650–658. [PubMed: 23797028]

Lin SL, Chien CW, Han CL, Chen ES, Kao SH, Chen YJ, Liao F. Temporal proteomics profiling of lipid rafts in CCR6-activated T cells reveals the integration of actin cytoskeleton dynamics. J. Prot. Res. 2010; 9:283–297.

Linder S, Aepfelbacher M. Podosomes: adhesion hot-spots of invasive cells. Trends Cell. Biol. 2003; 13:376–385. [PubMed: 12837608]

Linder S, Wiesner C. Tools of the trade: podosomes as multipurpose organelles of monocytic cells. Cell Mol. Life Sci. 2015; 72:121–135. [PubMed: 25300510]

Ma T, Sadashivaiah K, Chellaiah MA. Regulation of sealing ring formation by l-plastin and cortactin in osteoclasts. J. Biol. Chem. 2010; 285:29911–29924. [PubMed: 20650888]

Messier JM, Shaw LM, Chafel M, Matsudaira P, Mercurio AM. Fimbrin localized to an insoluble cytoskeletal fraction is constitutively phosphorylated on its headpiece domain in adherent macrophages. Cell Motil. Cytoskeleton. 1993; 25:223–233. [PubMed: 8221900]

Morley SC, Wang C, Lo WL, Lio CW, Zinselmeyer BH, Miller MJ, Brown EJ, Allen PM. The actin-bundling protein l-plastin dissociates CCR7 proximal signaling from CCR7-induced motility. J. Immunol. 2010; 184:3628–3638. [PubMed: 20194718]

Ning Y, Gerger A, Zhang W, Hanna DL, Yang D, Winder T, Wakatsuki T, Labonte MJ, Stintzing S, Volz N, et al. Plastin polymorphisms predict gender- and stage-specific colon cancer recurrence after adjuvant chemotherapy. Mol. Cancer Ther. 2014; 13:528–539. [PubMed: 24170770]

Pollard JW. Trophic macrophages in development and disease. Nat. Rev. Immunol. 2009; 9:259–270. [PubMed: 19282852]

Ray, A.; Dittel, BN. Isolation of mouse peritoneal cavity cells.. J. Vis. Exp. 2010. http://dx.doi.org/10.3791/1488

Riedl J, Crevenna AH, Kessenbrock K, Yu JH, Neukirchen D, Bista M, Bradke F, Jenne D, Holak TA, Werb Z, et al. Lifeact: a versatile marker to visualize F-actin. Nat. Methods. 2008; 5:605–607. [PubMed: 18536722]

Riedl J, Flynn KC, Raducanu A, Gartner F, Beck G, Bosl M, Bradke F, Massberg S, Aszodi A, Sixt M, et al. Lifeact mice for studying F-actin dynamics. Nat. Methods. 2010; 7:168–169. [PubMed: 20195247]

Riplinger SM, Wabnitz GH, Kirchgessner H, Jahraus B, Lasitschka F, Schulte B, van der Pluijm G, van der Horst G, Hammerling GJ, Nakchbandi I, et al. Metastasis of prostate cancer and melanoma cells in a preclinical in vivo mouse model is enhanced by l-plastin expression and phosphorylation. Mol. Cancer. 2014; 13:10. http://dx.doi.org/10.1186/1476-4598-13-10. [PubMed: 24438191]

Schneider CA, Rasband WS, Eliceiri KW. NIH Image to ImageJ: 25 years of image analysis. Nat. Methods. 2012; 9:671–675. [PubMed: 22930834]

Tachibana K, Hirota S, Iizasa H, Yoshida H, Kawabata K, Kataoka Y, Kitamura Y, Matsushima K, Yoshida N, Nishikawa S, et al. The chemokine receptor CXCR4 is essential for vascularization of the gastrointestinal tract. Nature. 1998; 393:591–594. [PubMed: 9634237]

Todd EM, Deady LE, Morley SC. The actin-bundling protein l-plastin is essential for marginal zone B cell development. J. Immunol. 2011; 187:3015–3025. [PubMed: 21832165]

Van Goethem E, Poincloux R, Gauffre F, Maridonneau-Parini I, Le Cabec V. Matrix architecture dictates three-dimensional migration modes of human macrophages: differential involvement of proteases and podosome-like structures. J. Immunol. 2010; 184:1049–1061. [PubMed: 20018633]

Williams LM, Ridley AJ. Lipopolysaccharide induces actin reorganization and tyrosine phosphorylation of Pyk2 and paxillin in monocytes and macrophages. J. Immunol. 2000; 164:2028–2036. [PubMed: 10657655]

Zhang X, Goncalves R, Mosser DM. Coligan, John E.The isolation and characterization of murine macrophages. Curr. Prot. Immunol. 2008; 11 Chapter 14, Unit 14.

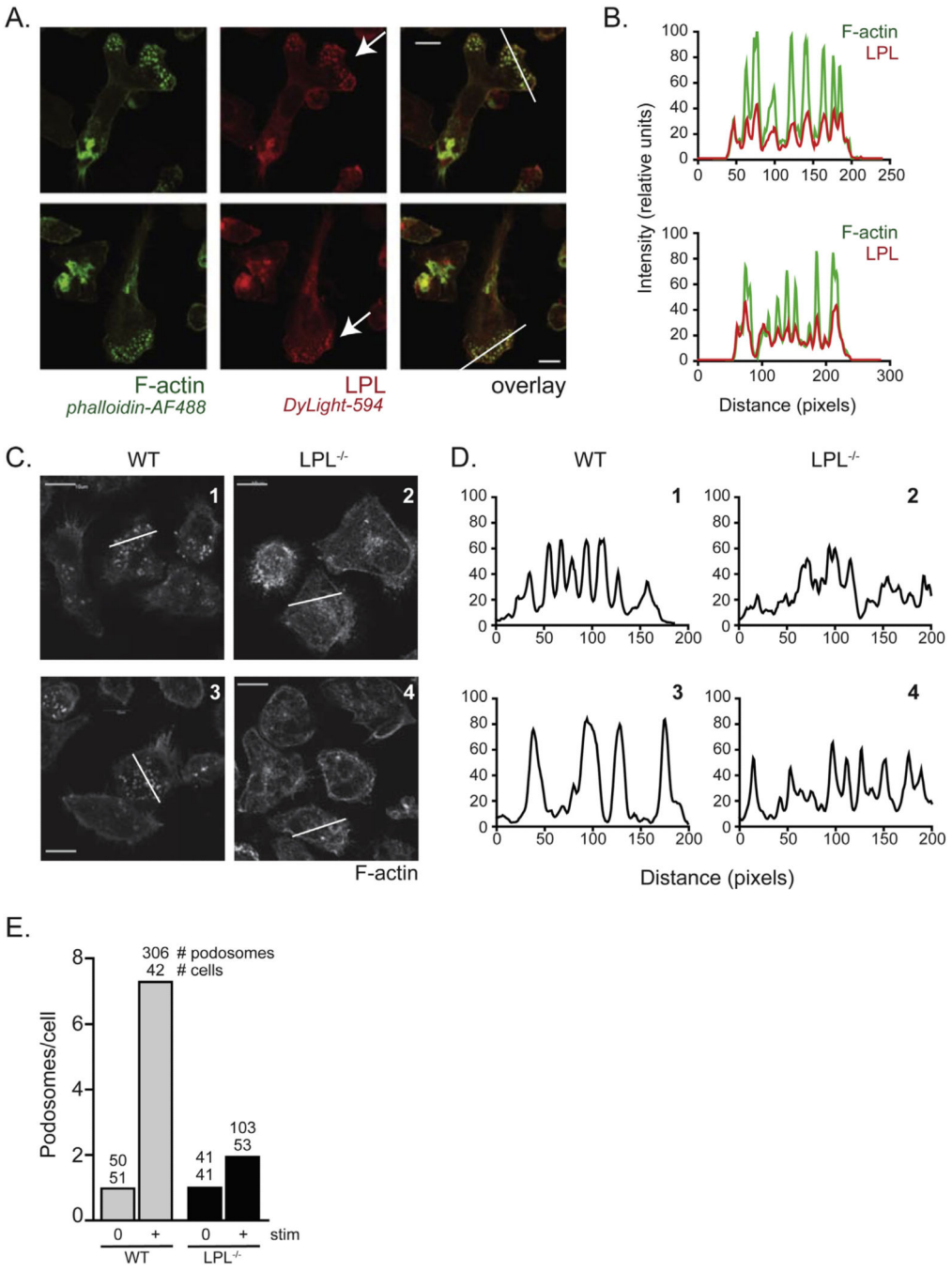

Fig. 1.

LPL is a key component of podosomes. A. Macrophages from thioglycollate-challenged WT mice were imaged for F-actin and LPL. Scale bar = 10 μm. B. Line scan intensity projections (thin white lines from panel A) reveal colocalization of LPL and F-actin. C. Confocal images of F-actin morphology of serum-stimulated peritoneal macrophages from naive WT or LPL$^{-/-}$ mice. Scale bar = 10 μm. D. Intensity of F-actin staining was projected along the line shown in (C) measured on a relative scale. Panel number indicates correlated image. E. Average number of podosomes per cell in peritoneal macrophages from WT and

$LPL^{-/-}$ mice with (+) or without (0) stimulation. Numbers above bars indicate total number of podosomes and cells counted. All cells in each randomly selected field were included unless cells were touching or the cells were not fully within the field. Results in panels A through E are representative of two independent experiments.

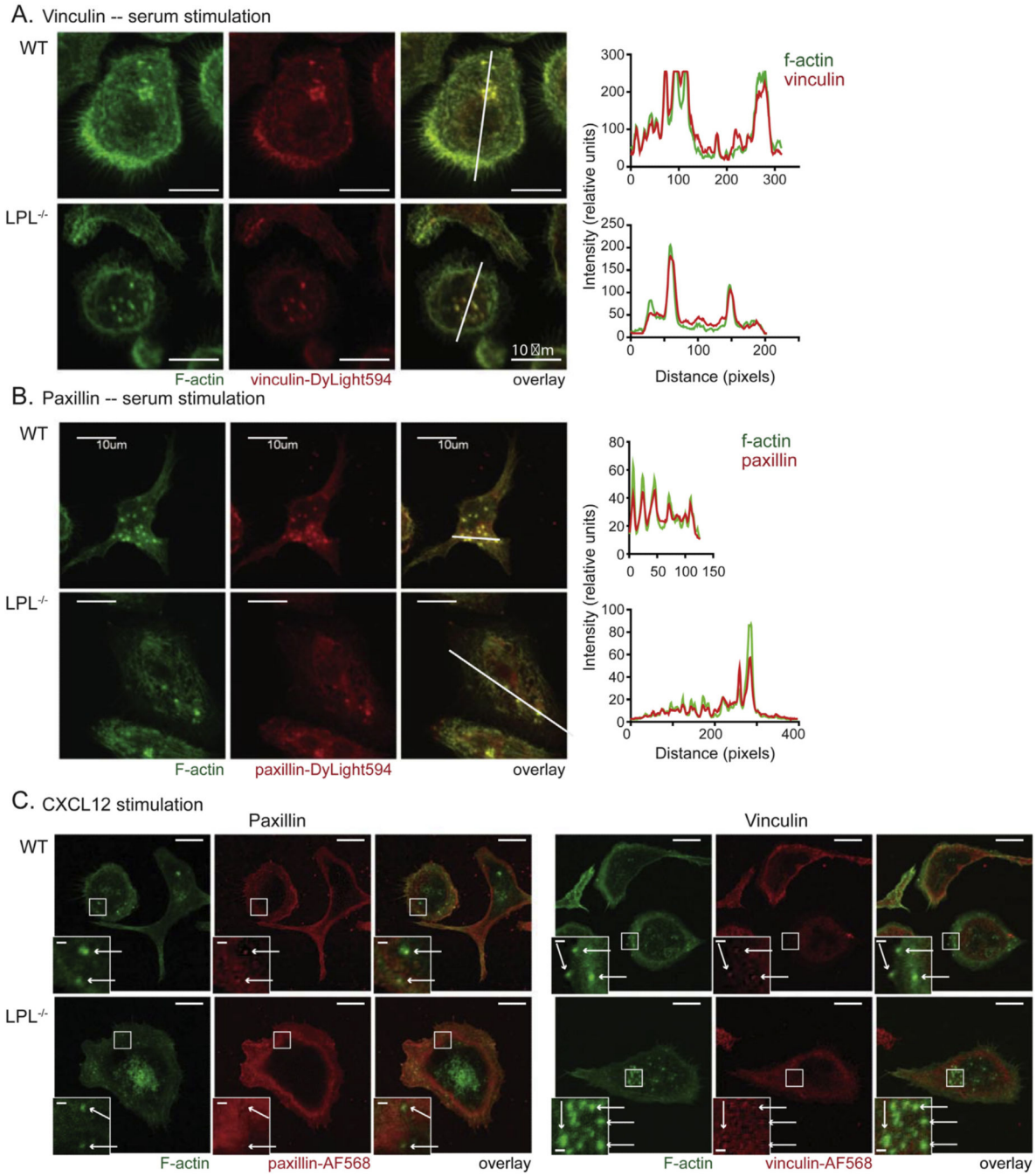

Fig. 2.

In peritoneal macrophages, colocalization of vinculin and paxillin with F-actin does not require LPL. A, B. Peritoneal macrophages derived from naive WT or LPL$^{-/-}$ mice were isolated, stimulated with serum/CCL2, fixed, and stained with phalloidin-AF488 and either anti-vinculin mAb (panel A) or anti-paxillin mAb (panel B). Relative intensity projections to the right were generated along the white lines in the images. Scale bar = 10 μm. Results are representative of at least 70 cells viewed in at least 12 fields of each condition from two independent experiments. C. Resident peritoneal macrophages derived from naive WT or

LPL$^{-/-}$ mice were isolated, stimulated with CXCL12, fixed, and stained with phalloidin-AlexaFluor488 and either anti-paxillin or anti-vinculin mAb followed by anti-IgG-AlexaFluor568. Insets represent approximately 4× magnification of the areas indicated by the small squares. Arrows indicate podosomes. Scale bar = 10 μm in larger panels; scale bar = 1 μm in insets.

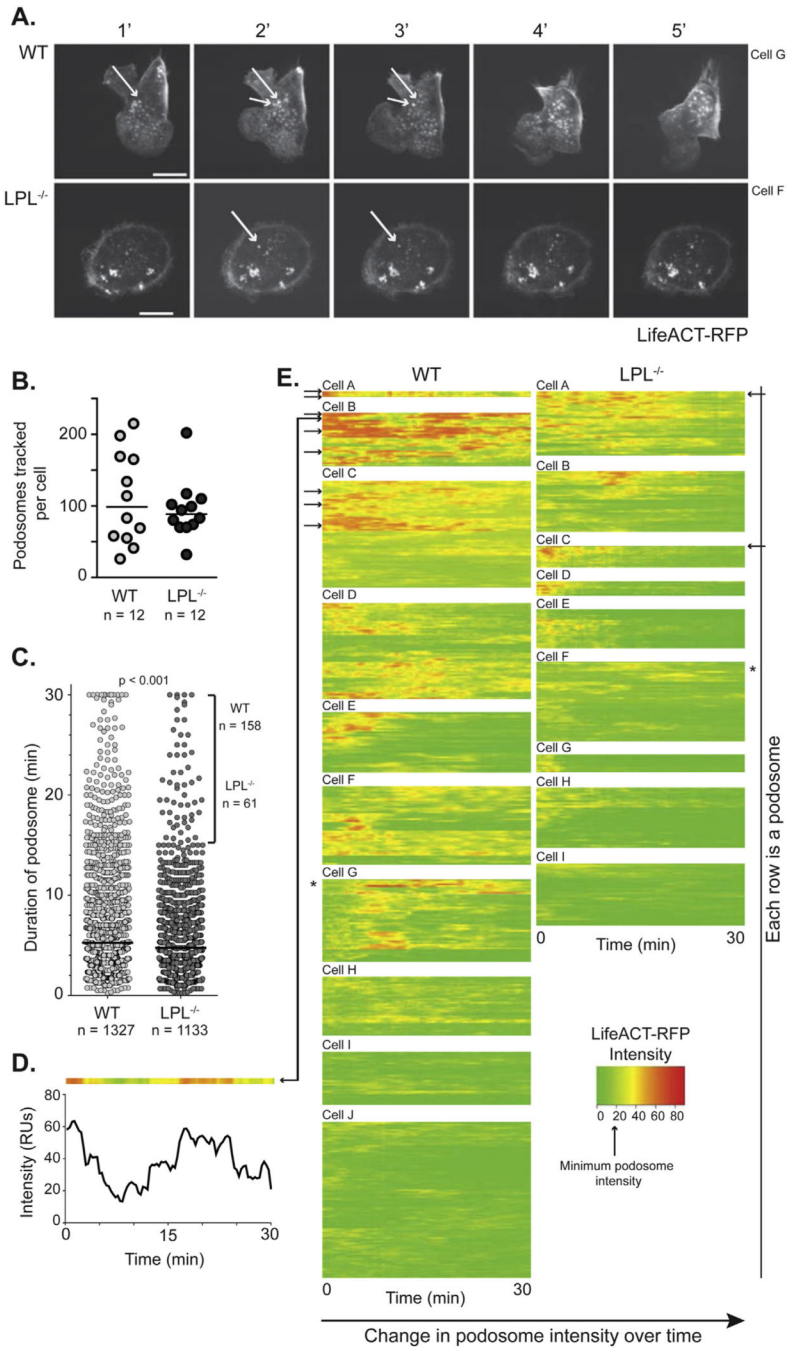

Fig. 3.

LPL supports podosome longevity. A. Peritoneal macrophages from naive LifeACT-RFP^{+}-WT and −LPL$^{-/-}$ mice were isolated, serum-starved, then re-stimulated and imaged for 30 min. Representative images are shown; see also Supplemental Movies 1 and 2. Arrows indicate examples of podosomes tracked over time. Heat maps of representative cells indicated by "*" in (D). Scale bar = 10 μm. B. Similar numbers of podosomes were observed and tracked in 12 cells from WT and LPL$^{-/-}$ mice. C. Duration of podosomes tracked in WT cells (median, 5.25 min) and LPL-deficient cells (median 4.75 min). Podosomes persisting at

the end of the 30-min imaging are clustered at the value of “30 min,” although the duration could be longer. D. Example of an oscillating podosome, with the fluorescence intensity profile displayed as a line graph of intensity vs time and also as a heat map, with intensity represented by a color scale. Arrow indicates position of representative podosome in the larger heat map. E. Heat maps show intensity (color scale) oscillations of podosomes formed in macrophages from WT and $LPL^{-/-}$ mice. Podosomes were defined as punctae with intensity values (~18.0 units) greater than that of the cell periphery (~13.5–14.5). Podosomes within each cell are clustered by intensity. Only podosomes that did not move from the point of origin for ≥6 frames are displayed in heat maps.

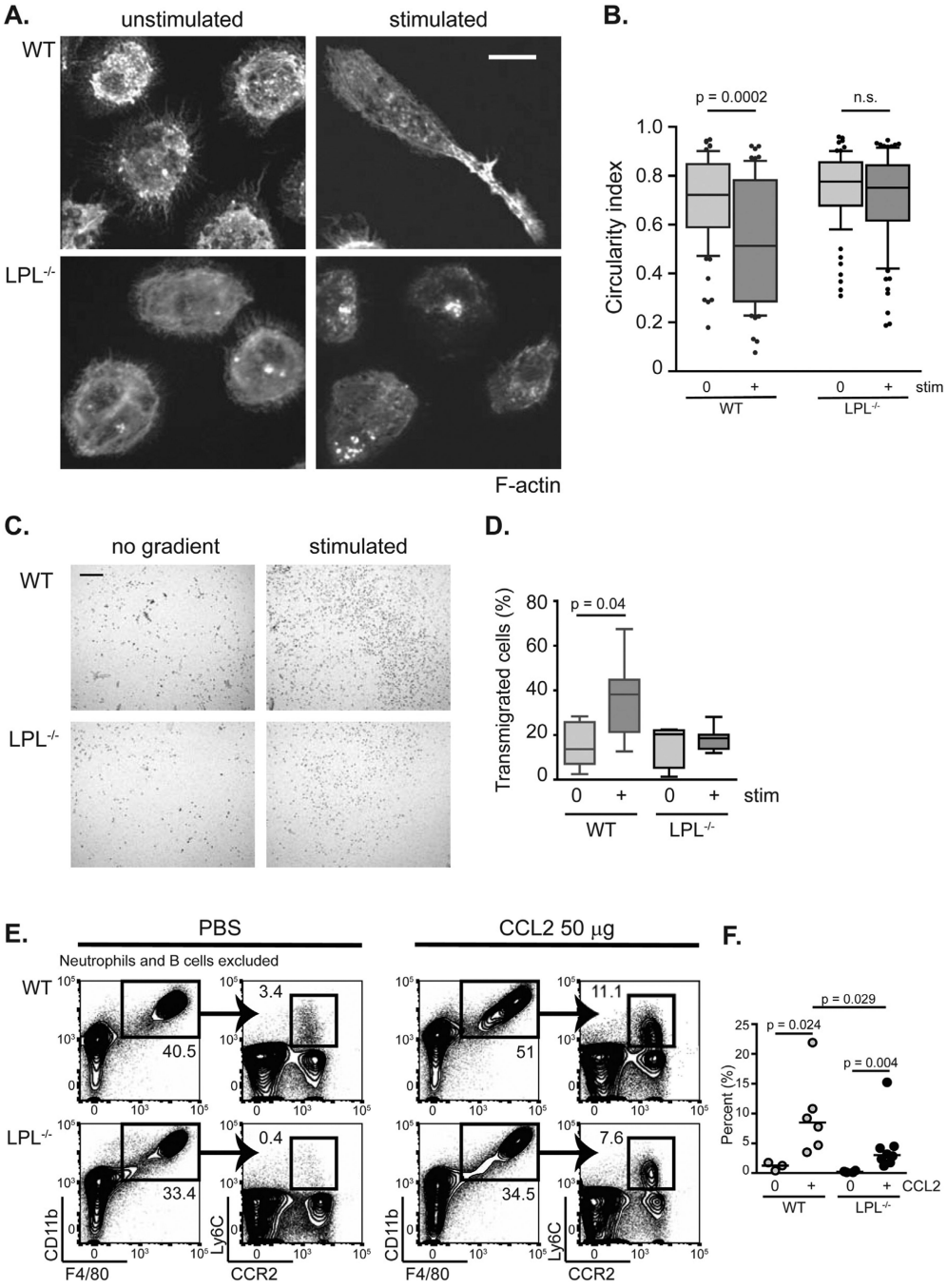

Fig. 4.

LPL is required for normal macrophage elongation and motility. A. Resident peritoneal macrophages from naive WT or LPL$^{-/-}$ mice were fixed after serum-starvation and restimulation (30 min). Scale bar = 10 μm. B. Circularity index of stimulated vs unstimulated macrophages from WT (gray circles) or LPL$^{-/-}$ (filled circles) mice, in which a value of "1" represents complete circularity. The middle line is the median, boxes show 25th–75th percentiles, whiskers show 10th–90th percentiles, and individual symbols represent outliers. The plot includes every cell (≥60 per group) from randomly selected

fields from two independent experiments. C. Resident peritoneal macrophages from WT and $LPL^{-/-}$ mice were plated on collagen-coated Transwell inserts and incubated overnight with or without a chemotactic gradient. Representative images of transmigrated cells shown. Scale bar = 200 μm. D. Percent of transmigrated cells determined by counting the number of cells on the Transwell before and after scraping the upper side. The center line is the median, the boxes show 25th–75th percentiles, whiskers show minimum and maximum. Data from four independent experiments. E. Representative flow cytometry from WT and $LPL^{-/-}$ mice 24 h after i.p. challenge with CCL2, with monocytes defined as $CD11b^{int}/Ly6C^{+}/CCR2^{+}$. F. Percentages of peritoneal cells that were monocytes. Each symbol represents one mouse, and the horizontal line indicates the median. Data acquired in three independent experiments.

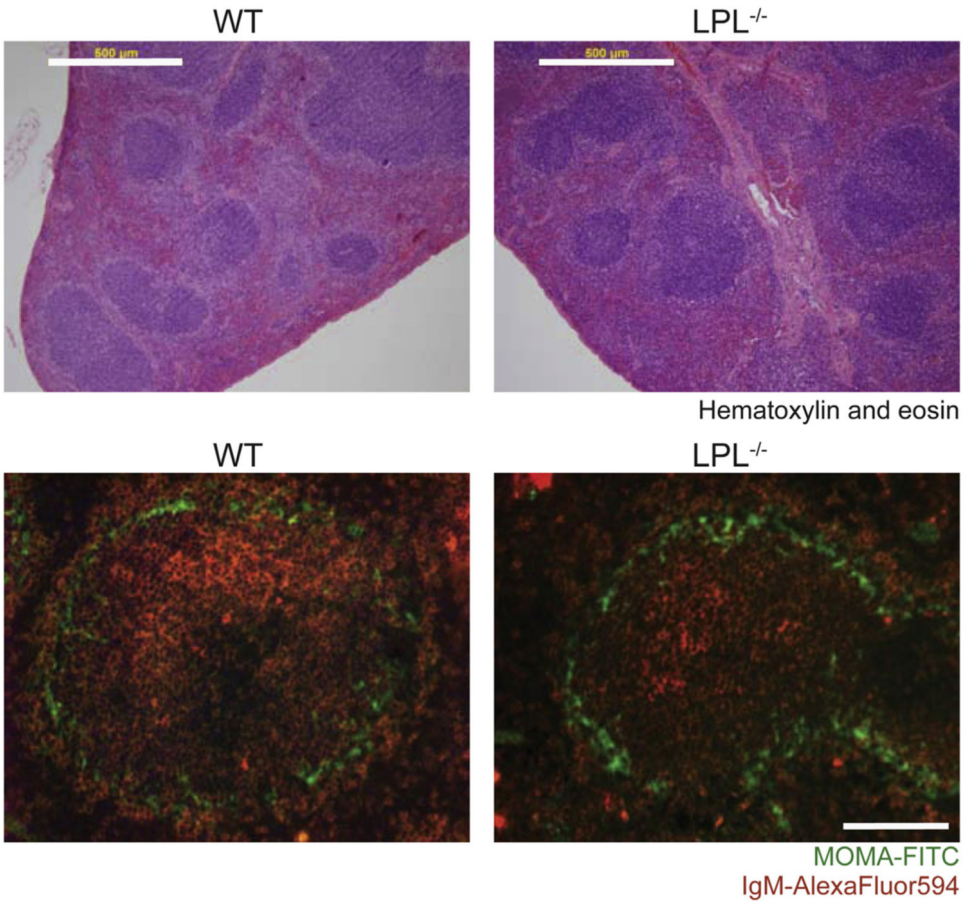

Fig. 5.

Splenic microarchitecture appears normal in LPL$^{-/-}$ mice. Spleens from WT and LPL$^{-/-}$ mice were fixed and imaged either by (A) hematoxylin and eosin staining or (B) immunofluorescence of marginal metallophilic macrophages (MOMA-1^{+}) and B cells (IgM^{+}) to reveal follicles. Scale bar indicates (A) 500 μm or (B) 100 μm. Representative of at least two independent experiments.